THE JOURNAL OF BIOLOGICAL CHEMISTRY VOL. 285, NO. 30, pp. 23224–23232, July 23, 2010

Structural Basis of Chaperone Recognition of Type III Secretion System Minor Translocator Proteins*[S]

Received for publication, February 5, 2010, and in revised form, April 6, 2010 Published, JBC Papers in Press, April 12, 2010, DOI 10.1074/jbc.M110.111278

Viviana Job[‡], Pierre-Jean Matteï[‡1], David Lemaire[§], Ina Attree[¶], and Andréa Dessen[‡2]

From the [‡]Bacterial Pathogenesis Group, Institut de Biologie Structurale, UMR 5075, CNRS/Commissariat à l'Enérgie Atomique/Université Joseph Fourier, 41 Rue Jules Horowitz, 38027 Grenoble, the [§]Laboratoire des Interactions Protéine Métal, IBEB, UMR 6191, CNRS/Commisariat à l'Enérgie Atomique/Université Aix-Marseille, 13108 Saint-Paul-lez-Durance, and [¶]UMR5092, CNRS, LBBSI, iRTSV, Commissariat à l'Enérgie Atomique, Université Joseph Fourier, 38054 Grenoble, France

The type III secretion system (T3SS) is a complex nanomachine employed by many Gram-negative pathogens, including the nosocomial agent *Pseudomonas aeruginosa*, to inject toxins directly into the cytoplasm of eukaryotic cells. A key component of all T3SS is the translocon, a proteinaceous channel that is inserted into the target membrane, which allows passage of toxins into target cells. In most bacterial species, two distinct membrane proteins (the "translocators") are involved in translocon formation, whereas in the bacterial cytoplasm, however, they remain associated to a common chaperone. To date, the strategy employed by a single chaperone to recognize two distinct translocators is unknown. Here, we report the crystal structure of a complex between the *Pseudomonas* translocator chaperone PcrH and a short region from the minor translocator PopD. PcrH displays a 7-helical tetratricopeptide repeat fold that harbors the PopD peptide within its concave region, originally believed to be involved in recognition of the major translocator, PopB. Point mutations introduced into the PcrH-interacting region of PopD impede translocator-chaperone recognition *in vitro* and lead to impairment of bacterial cytotoxicity toward macrophages *in vivo*. These results indicate that T3SS translocator chaperones form binary complexes with their partner molecules, and the stability of their interaction regions must be strictly maintained to guarantee bacterial infectivity. The PcrH-PopD complex displays homologs among a number of pathogenic strains and could represent a novel, potential target for antibiotic development.

The type III secretion system (T3SS)[3] is a complex, multiprotein structure that plays a key role in the infectivity process of a number of Gram-negative pathogens. The system serves as a conduit to inject T3SS-specific toxins directly into the cytosol of target cells, bypassing periplasmic and extracellular steps, required in the case of other bacterial secretion systems. The T3SS is composed of over 20 macromolecules that associate into a basal structure spanning both bacterial membranes and is terminated by a hollow needle through which toxins are thought to travel in semi-unfolded state (1–5). Toxin entry into the target cytoplasm requires the formation of a proteinaceous pore (the translocon) on the eukaryotic membrane; the translocon is generally composed of two T3SS-encoded membrane proteins (the hydrophobic translocators) and one hydrophilic partner (the V antigen) (6). In all systems studied to date, the largest of the hydrophobic translocators displays two predicted transmembrane regions (and henceforth will be called the major translocator, *i.e.* YopB in *Yersinia* spp., IpaB in *Shigella* spp., and EspD in *Escherichia coli* spp.), while the smallest protein (*i.e.* the minor translocator, YopD, IpaC, and EspB in the aforementioned organisms) carries a single predicted membrane-association region (7). Seven distinct families of T3SS have been identified; within them, macromolecules that compose base, needle, and translocon display sequence similarities not only at the genetic level but also in locus organization (8). However, toxins are pathogen-specific, and their distinct characteristics play key roles in the different intracellular consequences of their injection (9).

Most toxins, prior to their secretion through the T3SS needle, are maintained within the bacterial cytoplasm complexed to a dedicated chaperone. Interestingly, the two hydrophobic translocator proteins, in all human pathogenic species studied to date, are not recognized by two individual chaperones but rather share a common chaperone (10, 11). Grouping of T3SS chaperones according to the function of their partner molecules has led to the development of a classification system in which those that recognize effector molecules are "type I" chaperones, and partners of translocators are "type II" chaperones. A third class of chaperones (type III) recognize needle-forming proteins (1, 12). The stoichiometry of the association between the hydrophobic translocator proteins and their cognate chaperone is still a matter of controversy. Although most hydrophobic translocators have been shown to be able to bind to their chaperones independently from one another, it is unclear if this occurs through the formation of distinct binary complexes (in which the chaperone binds each translocator individually) or if the same chaperone binds both translocators simultaneously by using distinct binding sites (13–15). Interestingly, the latter suggestion is related to the hypothesis that both translocator

* This work was supported in part by a grant from the Commissariat à l'Energie Atomique "Transport de Protéines Membranaires" program (to A. D. and I. A.).

[S] The on-line version of this article (available at http://www.jbc.org) contains supplemental Figs. S1–S4.

The atomic coordinates and structure factors (codes 2xcb and 2xcc) have been deposited in the Protein Data Bank, Research Collaboratory for Structural Bioinformatics, Rutgers University, New Brunswick, NJ (http://www.rcsb.org/).

[1] Supported by a Ph.D. fellowship from the Cluster 10-Infectiologie/Rhône-Alpes Region.

[2] To whom correspondence should be addressed. Tel.: 33-4-38-78-95-90; Fax: 33-4-38-78-54-94; E-mail: andrea.dessen@ibs.fr.

[3] The abbreviations used are: T3SS, type III secretion system; TPR, tetratricopeptide repeat; A.U., absorbance units; LDH, lactate dehydrogenase.

proteins may travel through the T3SS needle in complexed form (15).

Recently, the structures of type II chaperones SycD from *Yersinia enterocolitica* and IpgC from *Shigella flexneri* have revealed that these molecules display tetratricopeptide (TPR)-like folds (16, 17). TPR-carrying domains are commonly involved in protein-protein interactions, are shaped like a cupped hand, and can employ both concave and convex regions for partner recognition; in addition, the concave region can bind to target molecules either as outstretched peptides (17) or helical arrangements (18). The identification of the binding site for a peptide from the *Shigella* major translocator IpaB within the concave region of the IpgC TPR-like fold confirmed that the TPR "palm" offers a binding platform for the major translocator (17). However, details regarding the interaction of a minor translocator protein with a T3SS type II chaperone remained unknown, and the stoichiometry of the complex(es) is also unclear.

The T3SS locus of *Pseudomonas aeruginosa*, a human pathogen responsible for nosocomial infections and major complications in cystic fibrosis patients, encodes two translocator proteins: the major translocator PopB (392 amino acids) and the minor translocator PopD (295 residues), which display very low sequence identity (19–21). PopB and PopD are expressed from the *pcrVGHpopBD* operon and are recognized and stabilized within the bacterial cytoplasm by the same chaperone, PcrH. Induction of the *P. aeruginosa* T3SS causes both PopB and PopD to be targeted to the eukaryotic membrane, where they participate in the formation of a pore whose internal diameter (2.8–3.5 nm) resembles that of the T3SS needle (19). It is of interest that *in vitro* both PopB and PopD form oligomers that, in the presence of lipids, generate ring-like structures (20) and work in concerted fashion toward pore formation (21).

Here, we have used a combined approach to elucidate the functional and structural properties of interactions between PcrH and the minor translocator PopD of the *P. aeruginosa* T3SS. In the absence of one of the translocator partner molecules, PcrH undergoes a monomer-dimer equilibrium that is only shifted toward the monomeric state by interaction with PopD. The high resolution structure of PcrH in complex with a peptide from the N terminus of PopD unexpectedly reveals that it occupies the concave region of the TPR fold of the chaperone, originally believed to be the binding site exclusively for the major translocator. Mutagenesis of PopD residues identified in the crystal structure as being anchor points within PcrH compromises PopD intracellular stability, prevents its secretion, and blocks *Pseudomonas* cytotoxicity toward macrophages. These results show that T3SS type II chaperones employ the same concave region of their TPR-like fold to bind both major and minor translocator molecules. The commonality of the TPR fold for translocator chaperones sheds light on a general mechanism of translocator stabilization within the bacterial cytoplasm prior to secretion through the T3SS needle.

EXPERIMENTAL PROCEDURES

Expression and Purification of Recombinant Proteins—The section of the *P. aeruginosa* CHA *pcrH* gene coding for amino acids 1–160 (or 21–160) was amplified using conventional PCR methodologies and cloned into vector pETDuet-1 (Novagen). Both clones contained an additional thrombin site, allowing for cleavage of the His tag upon protein purification. PcrH(21–160), used for crystallization experiments, was expressed in *E. coli* BL21(DE3), and PcrH(1–160) was expressed in *E. coli* BL21(DE3)pLysS. Cultures were grown at 37 °C to $A_{600\ nm}$ of 0.7 A.U., and expression of the recombinant proteins was induced by the addition of 1 mM isopropyl 1-thio-β-D-galactopyranoside for 3.5 h at 30 °C. Cells were lysed on ice by sonication in 25 mM Tris-HCl, pH 8.0, 0.2 M NaCl, 5% glycerol, in the presence of protease inhibitors (Roche Applied Science) and then centrifuged at 30,000 × *g* for 45 min. The supernatant was applied to a HisTrap HP 5-ml column (GE Healthcare) washed with 25 mM Tris-HCl, pH 7.4, 0.2 M NaCl, 20 mM imidazole, 5 mM β-mercaptoethanol, and the bound proteins were eluted with a linear gradient of the same buffer containing 500 mM imidazole. Prior to thrombin cleavage, proteins were dialyzed into 25 mM Tris-HCl, pH 8.0, 0.1 M NaCl for 1 h. Cleaved products were loaded onto a His trap column to eliminate the uncleaved fractions and subsequently onto a Superdex 200 column previously equilibrated in 20 mM Tris-HCl, pH 8.0, 0.1 M NaCl, 2 mM EDTA, 10% glycerol, and 3 mM dithiothreitol.

Clone PcrH(21–160) required the presence of 0.5 M NaCl during purification; in addition to the steps described above, the protein was further purified by Mono Q (GE Healthcare) using a linear gradient of 0.5 M NaCl in 25 mM Tris-HCl, pH 8.0, 1 mM EDTA, and 5 mM dithiothreitol.

Subsequently, full-length *popD* (coding for residues 1–295) was cloned into the second multiple cloning site of the PcrH-carrying pETDuet-1 plasmid (described above). The plasmid was transformed into *E. coli* BL21(DE3)pLysS, and protein expression was performed with 1 mM isopropyl 1-thio-β-D-galactopyranoside at 16 °C overnight. The His_6-PcrH(1–160)-PopD complex was eluted in 75 mM imidazole from a HisTrap column and dialyzed in 25 mM Tris-HCl, pH 8.0, 1 mM EDTA, 10% glycerol prior to being submitted for gel filtration experiments as described above.

Analytical Gel Filtration—PcrH(1–160) and the His_6-PcrH(1–160)-PopD complex were concentrated to 100 and 30 mg/ml, respectively. Sequential dilutions were performed on the samples and subsequently loaded on a Superdex 200 10/300 (GE Healthcare) column equilibrated in 20 mM Tris-HCl, pH 8.0, 0.1 M NaCl (in the presence or absence of 10% glycerol and 2 M NaCl). For evaluation of the Stokes radius (R_S) and calculation of the apparent molecular mass of the samples, the column was calibrated in each buffer using albumin (67 kDa, R_S = 35.3Å), ovalbumin (43 kDa, R_S = 30.5Å), chymotrypsinogen A (25 kDa, R_S = 20.9Å) and ribonuclease A (13.7 kDa, R_S = 16.4Å).

Crystallization, Data Collection, and Structure Solution—PcrH(21–160) was concentrated to 33 mg/ml, and an initial screening was performed using the high throughput crystallization platform (HTXLab; PSB, Grenoble, France) at 4 °C. Crystals were produced in 0.1 M Tris-HCl, pH 8.5, 0.2 M $MgCl_2$, and 15% PEG4000. Crystals were cryoprotected by successive brief incubations in mother liquor containing increasing concentrations in glycerol (up to 20%) and were subsequently flash-

cooled in liquid nitrogen. Data collection was performed on the ID14-EH2 beamline at the ESRF (Grenoble, France) and subsequently processed and scaled with XDS (22).

The structure was solved by molecular replacement using PHASER (23). A truncated form of SycD (Protein Data Bank code 2VGX), including residues 36–137, was used as a search model. To eliminate bias, all residues that were different between SycD and PcrH were mutated into alanines prior to molecular replacement. Cycles of automatic and manual building were performed using REFMAC 5.4 (24) and Coot (25). For the PcrH-PopD complex, PcrH(21–160) at 30 mg/ml was mixed with a synthetic peptide whose sequence corresponded to residues 47–56 of PopD (DRVELNAPRQ, prepared in 100% DMSO) at a 1:2 molar ratio in the presence of 40 mM dithiothreitol and 40 mM Tris-HCl, pH 8.5. Crystals grew in 1 day at 4 °C in 0.1 M Tris-HCl, pH 8.0, 1.5 M LiCl, 16% PEG6000. Crystals were cryoprotected as described for the native PcrH crystals, directly on the beamline. Data collection was performed at the ESRF (beamline ID14EH2), and data processing and scaling were performed using the programs described above. The structure was solved with PHASER by employing the structure of native PcrH as a search model. Refinement was performed with REFMAC5 and Coot. Structure geometry was analyzed with Molprobity (26). Structure figures were generated with PyMOL (3).

Mass Spectrometry—Noncovalent mass spectrometry measurements of PcrH were performed by using a Q-TOF micro mass spectrometer (Waters) with an electrospray ion source. Mass spectra were recorded in the 2000–5000 mass-to-charge (*m/z*) range. Sample concentration was 20 μM in 20 mM ammonium bicarbonate and continuously infused at a flow rate of 7 μl/min. Mass spectra were acquired, and data were processed with MassLynx 4.0 (Waters). In both cases, data were acquired in the positive mode, and calibration was performed using a solution of 0.1 mg/ml CsI in water/isopropyl alcohol (1:1, v/v).

Dynamic Light Scattering—Light scattering measurements were performed in a 90° angle light scattering instrument (DynaPro, Protein Solutions). PcrH(1–160) was tested at final concentrations ranging between 60 and 110 mg/ml in 25 mM Tris-HCl, pH 8.0, 0.1 M NaCl, 1 mM EDTA, with or without 10 mM dithiothreitol and 10% glycerol. Approximately 12 replicate measurements were collected and averaged. The results were analyzed with the Dynamics 4.0 Software.

Generation of Mutant P. aeruginosa Strains—All mutagenesis reactions were performed following the protocol described in the QuikChange® II site-directed mutagenesis kit (Stratagene), except that DMSO (in a range of 4–6%) was added to the mixtures. The four 57-bp primers were designed to introduce, with a single PCR, either three mutations E50R, N52A, and R55E (PopD-RAE mutant), or four mutations V49D, L51D, A53D, and P54D (PopD-4D mutant). The same primers were used with both vectors used in this work: pETDuet-*6His-pcrHpopD* (27) used for *in vitro* assays, and pIApG-*pcrHpopBD* (20) used for all the *in vivo* experiments. The presence of mutations was confirmed by DNA sequencing.

Protein Expression, Secretion, and Stability Assays—*P. aeruginosa* strain CHA depleted from both *popB* and *popD* genes (Δ*popBD*) was transformed with the three pIApG-*pcrHpopBD* vectors harboring PopD wild type, PopD-4D, or PopD-RAE sequences. All cultures were performed at 300 rpm in Luria Bertani medium in the presence of 200 μg/ml carbenicillin, 20 mM $MgCl_2$, and 5 mM EGTA to induce the T3SS. For protein expression and secretion, the pellet and supernatant of a *Pseudomonas* culture at A_{600} = 1.0 A.U. were analyzed. A volume corresponding to 100 μl of a *Pseudomonas* culture (for expression tests) and 10 μl of the supernatant (for secretion tests) was loaded on a 15% SDS-PAGE and subsequently analyzed by Western blotting. Protein stability was analyzed by the addition of 500 μg/ml chloramphenicol to a *Pseudomonas* culture (A_{600} = 1.0 A.U.) grown in T3SS-inducing conditions. At 1–3 h after protein synthesis had been blocked, 100 μl of the expression fractions were loaded on each SDS-PAGE lane. Immunoblotting was carried out using rabbit antibodies directed against PcrH (diluted 1:1000), PopD (diluted 1:1000), PopB (diluted 1:5000), and PcrV diluted (diluted 1:3000).

Cytotoxicity Assays—To test the functionality of the T3SS in the PopD mutants, the cytotoxicity toward the macrophage cell line J774 was determined. 2.5×10^5 macrophages were grown in a 48-well plate and infected with *Pseudomonas* cultures (A_{600} = 1.0 A.U.) at a multiplicity of infection of 50. 30-μl aliquots were taken after 1 and 3 h, and the release of the lactate dehydrogenase from the infected cells was quantified with the LDH cytotoxicity infection kit (Roche Applied Science). The 100% cytotoxicity value was determined with 5% Triton X-100, and noninfected macrophages were taken as negative control.

RESULTS

Binding of the PopD Translocator to PcrH Stabilizes Its Oligomeric State—T3SS class II chaperones recognize two translocator proteins (10, 11), and both in *Yersinia* and *Shigella* spp. have been shown to form homodimers in solution and require dimerization for activity (16, 17). To determine whether PcrH also undergoes dimer formation in the presence and absence of Pop molecules, we determined the oligomeric state of the bound and unbound forms of tagless PcrH(1–160) (henceforth called PcrH) by gel filtration at different protein concentrations as well as by native mass spectrometry and dynamic light scattering. In size exclusion chromatography experiments, PcrH concentrations above 5 mg/ml (up to 83 mg/ml) yielded profiles in which the protein eluted between molecular mass markers 25 and 43 kDa (thus, with a potential molecular mass of 41 kDa, with Stokes radii in the range of 28 Å), suggesting the formation of a dimer (Fig. 1*A*, *solid line*). The dimeric nature of concentrated PcrH samples was confirmed by dynamic light scattering measurements, which suggested values ranging from 26.7 to 35.4 kDa (with corresponding Stokes radii ranging between 25.0 and 28.2 Å). Notably, however, sample concentrations lower than 5 mg/ml yielded profiles corresponding to an equilibrium between monomeric and dimeric forms (Fig. 1*A*, *dashed line*), whereas at very low protein concentrations (0.1 mg/ml) the profile resembled that of a monomeric species (Fig. 1*A*, *dotted line*). This was confirmed by a native mass spectrometry experiment in which PcrH at 0.8 mg/ml yielded two major peaks, at 17,741.5 ± 0.2 and 35,481.4 ± 0.4 Da (theoretical mass of the monomer, 17,744 Da). Comparable results were obtained by mass spectrometry, gel filtration, and chemical cross-linking

with PcrH in which the His tag was not cleaved, as well as with a PcrH form lacking the N-terminal region (PcrH(34–160)), previously identified by limited proteolysis (data not shown and see Ref. 27). This suggests that although PcrH can exist in two distinct quaternary states, its N terminus does not play a role in the dimerization process, a behavior that is distinct from what has been observed for other type II chaperones of the T3SS.

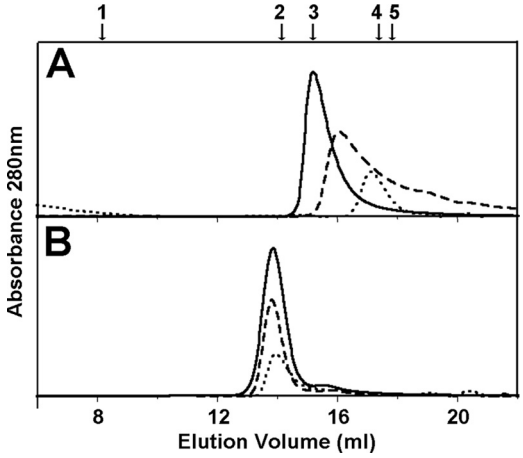

FIGURE 1. **PcrH displays a monomer-dimer equilibrium, except when associated to PopD.** *A,* gel filtration profiles of PcrH at 8.3 mg/ml (*solid line*), 0.8 mg/ml (*dashed line*), and 0.08 mg/ml (*dotted line*). *B,* gel filtration profiles of PopD-PcrH at 3.3 mg/ml (*solid line*), 0.33 mg/ml (*dashed line*), and 0.033 mg/ml (*dotted line*). Molecular mass standards employed were as follows: *1,* blue dextran; *2,* albumin (67 kDa); *3,* ovalbumin (43 kDa); *4,* chymotrypsinogen A (25 kDa); and *5,* ribonuclease A (13.7 kDa).

Subsequently, a His_6-PcrH(1–160)-PopD sample was prepared from an *E. coli* extract expressing both proteins from a bicistronic construct (20). When the sample containing both proteins was submitted to analytical size exclusion chromatography, the complex always eluted as a single peak in the proximity of the 67-kDa marker (albumin), irrespective of the protein concentration (Fig. 1*B*) or of buffer conditions employed (supplemental Fig. S1). This elution volume suggests an approximate Stokes' radius of 35.2 Å, corresponding to a mass of 62.2 kDa. These values are in agreement with the 1:1 stoichiometry identified previously by native mass spectrometry (20) and suggest that PopD binding "locks" PcrH in a complex where it remains in monomeric state. Notably, a 1:1 PopB-PcrH complex could not be stably isolated due to the high tendency of PopB to form mixtures of oligomers (data not shown).

PcrH Displays a 7-Helical TPR-like Fold—To gain insight into the PcrH fold and potentially its interaction with T3SS translocators, we initially sought to crystallize PcrH in its apo-form. Because crystals of the form harboring residues 1–160 of PcrH could not be obtained, we used limited proteolysis with thrombin to identify a stable domain. Digestion was followed by SDS-PAGE and mass spectrometry and identified that a stable form of PcrH, lacking the 20 first amino acids, could be obtained after 1 h. This PcrH variant (residues 21–160) was subsequently expressed and shown by gel filtration to display the same monomer-dimer equilibrium as the native molecule (data not shown). PcrH(21–160) crystallized in space group $P2_1$, with two monomers in the asymmetric unit. Data were collected to 2.13 Å at the ESRF Synchrotron (Grenoble, France), and the structure of PcrH was solved by molecular replacement using a polyalanine model of the SycD structure (Protein Data Bank code 2VGX) as a search model.

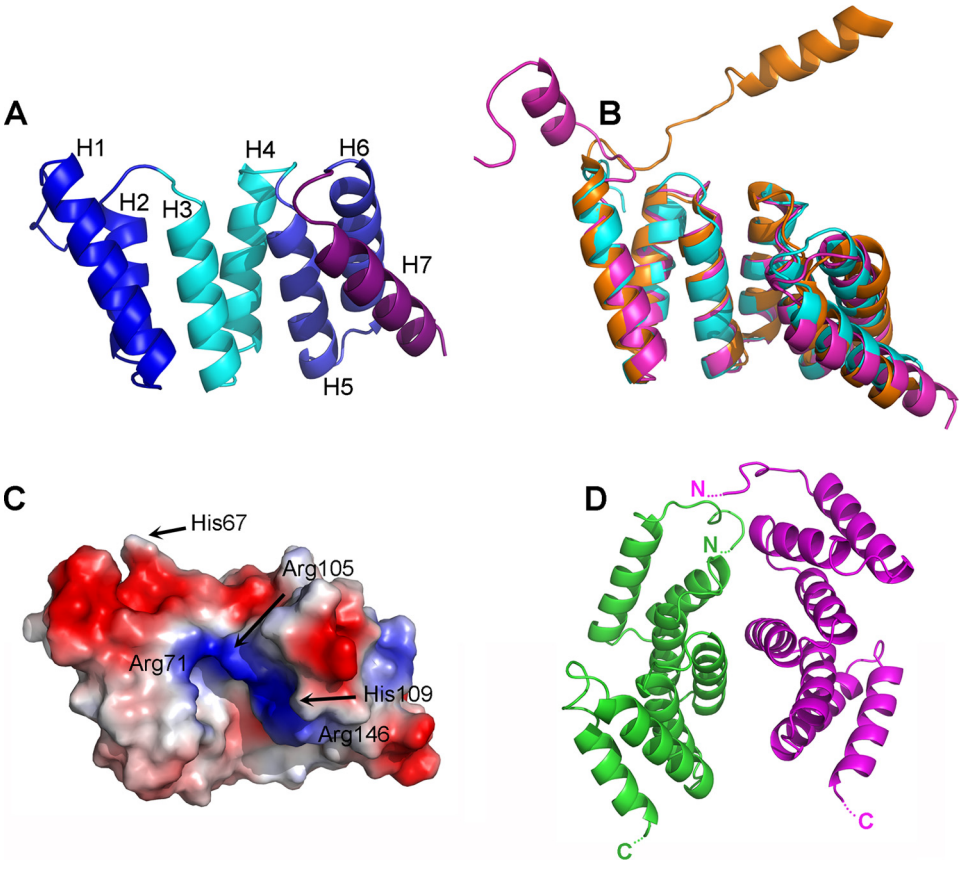

FIGURE 2. *A,* PcrH(21–160) displays a 7-helical TPR-like fold. Each one of the TPR domains is shown in a different color, with helix 7 in *violet*. *B,* superposition of IpgC (*orange*), SycD (*pink*), and PcrH (*cyan*) reveals very similar overall folds, with differences mostly at the N termini. *C,* PcrH displays a highly charged surface. Indicated residues point directly into the concave cleft and interact with the partner molecule. *D,* dimer interactions are made through the convex side of the TPR fold of PcrH.

The overall structure of PcrH(21–160) is shown in Fig. 2*A*; it displays an all-helical tetratricopeptide fold with three TPR-like motifs, each composed of two α-helices; one additional α-helix is present at the C terminus (helix 7 in Fig. 2*A*). This helical arrangement is reminiscent of the folds of SycD and IpgC, the chaperones for the translocator proteins from *Yersinia* and *Shigella* spp., respectively (16, 17), as well as that of PscG, the 7-helical chaperone of the *P. aeruginosa* T3SS needle-forming protein PscF (18). A

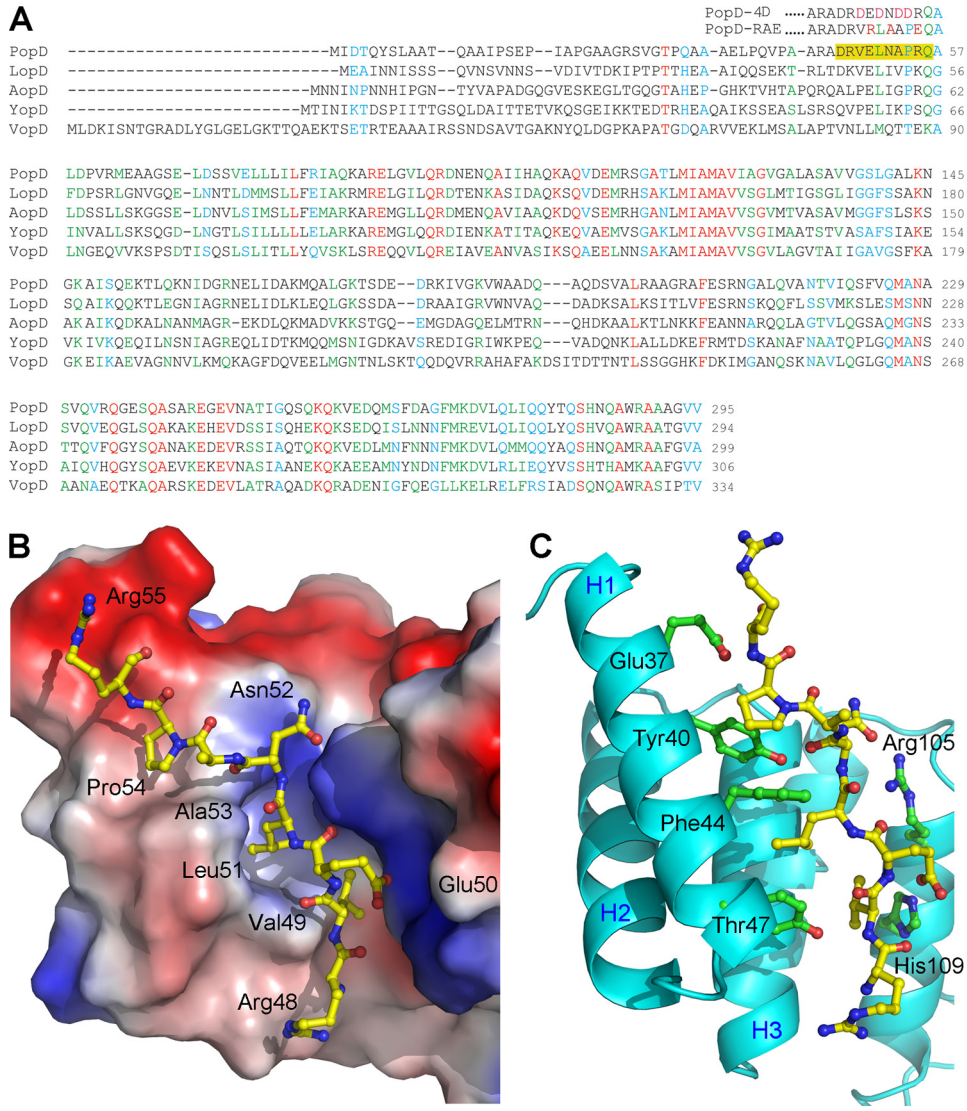

FIGURE 3. *A,* sequence alignment of minor translocon molecules of bacteria harboring T3SS in the Ysc/Psc family. Sequences include PopD (*P. aeruginosa*), LopD (*Photorhabdus luminescens*), AopD (*Aeromonas hydrophila*), YopD (*Y. pestis*), and VopD (*Vibrio harveyi*). *Green* and *blue* residues display strong/weak similarities, respectively, as determined by ClustalW. Identical residues are indicated in *red*. The sequence that corresponds to the region selected for crystallization studies is highlighted in *yellow*, and those of the mutants studied in this work are shown above the alignment. *B,* PopD(47–56) is located snugly within the charged PcrH concave cleft. Two hydrophobic residues, Val-49 and Leu-51, anchor PopD deeply into the binding site. *C,* details of the PcrH-PopD interactions. A number of residues from H1, H3, and H5 (in *green*) interact directly with the peptide, which is shown in *yellow*. The view has been slightly rotated with respect to *B* to facilitate analysis.

comparison of the structures of PcrH, SycD, and IpgC reveals high structural similarities within the core of the TPR domains, whereas the N termini of the molecules diverge (Fig. 2*B*). The flexibility of the N termini of different type II chaperones could potentially explain our difficulty in obtaining crystals of the full-length form of PcrH (see below). In PcrH, helices H3, H4, and H5 form the central part of the highly charged concave region (Fig. 2, *A* and *C*). Two potential dimeric arrangements are observed; the one with the most interactions, observed in the asymmetric unit, is formed by apposition of the convex surfaces of the monomers (Fig. 2*D*). There are very few interactions between the two monomers; Tyr-95, Leu-98, and Met-99, located on the C terminus of H4, were solely responsible for contacting H2 and H4 residues in the neighboring monomer. A second potential dimeric arrangement was observed between monomers of different asymmetric units that interact through the PcrH N terminus, albeit also making few contacts; this association is distinct from that observed for other TPR-harboring chaperones (supplemental Fig. S2). These observations were in agreement with the size exclusion chromatography data, which revealed that, in the absence of a partner, PcrH can be stabilized as a dimer at high concentrations but remains monomeric in low amounts of protein.

PcrH Palm Recognizes a Specific PopD Sequence—Interaction between PcrH and minor translocator PopD generates a 1:1 complex, thus blocking PcrH in monomeric form (Fig. 1*B*), but no structural information regarding this type of complex was available. Our earlier study of the PopD-PcrH complex had identified that PopD displays molten globule characteristics both in the absence and presence of PcrH, and limited proteolysis of the PopD:PcrH 1:1 complex revealed that PopD residues 28–95 were able to associate with PcrH and still maintain a 1:1 stoichiometry (27). Subsequently, Lunelli *et al.* (17) identified a short region in the *Shigella* major translocator protein IpaB (^{65}PELKAP^{70}) that specifically recognizes its type II chaperone, IpgC. By analyzing sequences of minor translocator proteins from T3SS of the Ysc family (8) and employing the IpaB peptide as a comparison criterium, we identified a potentially minimal PopD-PcrH interacting region (PopD residues 49–54, VELNAP) that maps to the PopD region identified by proteolysis (Fig. 3*A*) (27).

We then incubated PcrH(21–160) with a synthetic peptide corresponding to the PopD sequence ^{47}DR**VELNAP**RQ^{56} and tested complex formation by native mass spectrometry. Five mass values could be identified as follows: apo, monomeric PcrH (15,470.8 ± 2.0 Da); apo, dimeric PcrH (30,942 ± 3.0 Da); a 1:1 PcrH-PopD(47–56) complex (16,668.3 ± 2.0 Da); a 2:2 complex (32,139.2 + 3.0 Da), and a 2:1 complex (33,334.3 ± 3.0 Da). These results were indicative of our capability to isolate a stable PcrH-PopD(47–56) complex; samples were submitted to high throughput crystallization trials, which generated crystals in both hexagonal ($P6_122$) and orthorhombic ($P2_12_12$) forms. Structures were solved to 1.8 Å by using apo-PcrH as a search model in molecular replacement experiments that identified

TABLE 1
Data collection, molecular replacement and structure refinement statistics

Data set	Native	PcrH-peptide complex
Data collection		
Wavelength	0.933 Å	0.933 Å
Space group	$P2_1$	$P2_12_12$
a	53.9 Å	44.4 Å
b	46.2 Å	97.7 Å
c	65.6 Å	73.6 Å
β	103.8°	
Resolution (last shell limits)	2.13 Å (2.26-2.13 Å)	1.85 Å (1.96-1.85 Å)
No. observed/unique reflections	89,026/15,766	384,040/28,174
Completeness	89.0% (65.8%)	99.8% (99.4%)
R_{meas} (last shell)	5.3 (47.5)	7.3 (58.6)
Resolution (Å)		
R_{mrgd}-*F* (last shell)	7.0 (44.4)	5.5 (33.1)
$I/\sigma(I)$ (last shell)	30.3 (3.9)	23.2 (4.7)
Refinement		
Resolution	2.13 Å	1.85 Å
R_{work}	25.78%	22.99%
R_{free}	29.61%	26.22%
No. of protein atoms	2,129	2,193
No. of solvent atoms	27	85
Root mean square deviation, bond lengths	0.017 Å	0.023 Å
Root mean square deviation, bond angles	1.71°	1.85°
Mean *B* factor	41.2 Å^2	32.5 Å^2
Wilson *B* factor	46.5 Å^2	35.7 Å^2
Molprobity output scores		
Ramachandran outliers (no. of residues/total residues)	4/261	1/267
Ramachandran favored (no. of residues/total residues)	236/261	265/267

that both crystal forms displayed PopD(47–56) bound to PcrH. Data collection and structure solution statistics are included in Table 1; only the orthorhombic form will be further discussed.

Calculation of a difference Fourier map ($F_o - F_c$) identified density within the concave region of subunit A of PcrH, allowing the unambiguous placement of PopD(47–56) within the "cupped palm" of the PcrH structure (Fig. 3*B*; supplemental Fig. S3). PopD residues 48–55 are clearly traceable, whereas Asp-47 and Gln-56 display poorly traceable side chain density. PopD(47–56) binds in extended form, with residues Val-49 and Leu-51 anchoring deeply into the concave chaperone cleft. PcrH residues Phe-44, which are located on H1, as well as Leu-74 and Ala-78, which line H3, provide the bulk of the hydrophobic interactions, which stabilize the PopD anchor residues. PopD residues Arg-48, Glu-50, and Asn-52, although not pointing into the PcrH cavity, do make interactions with polar residues within the concave cleft, namely Tyr-40, Tyr-47, Arg-105, and His-109 (Figs. 2*A* and 3*C*).

This was an unexpected result, because mutagenesis experiments based on three-dimensional models of SycD and PcrH suggested that the concave cleft of the type II chaperones contains the binding site for the major, and not the minor, translocator protein (13, 14). Thus, the structure of the PcrH-PopD(47–56) complex presented here reveals that the concave region of the type II chaperone TPR fold can bind specific regions from both major and minor translocator proteins, which can presumably then wrap around the chaperone in distinct fashions. It is of interest, however, that a comparison between the structure of the PcrH-PopD(47–56) (this work) and IpgC-IpaB(60–72) (17) reveals that both major and minor translocator sequences are accommodated within their respective chaperone clefts in a very similar fashion (supplemental Fig. S4). The peptides interact mostly with residues from the two central helices in both chaperones; the two anchors in the present structure, Val-49 and Leu-51, of PopD, correspond to Pro-65 and Leu-67 in IpaB, which also point deeply into the IpgC cleft. These results thus suggest that, in different bacterial species, both T3SS hydrophobic translocators utilize the concave region of their common chaperone as a key recognition region.

PopD Hydrophobic Residues Are Essential for T3SS-induced Cytotoxicity—To confirm that the ^{49}VELNAP^{54} motif plays a role in Pop functionality and PcrH recognition, we modified the highly cytotoxic *P. aeruginosa* CHA strain (originally isolated from a cystic fibrosis patient) to carry mutations in this motif in PopD, and we tested these mutants for T3SS-dependent cytotoxicity in a cellular model of infection. A mutant strain carrying a PopD variant with point mutations in the ^{49}VELNAP^{54} region, in which the four hydrophobic residues of the motif were replaced by Asp (^{49}DEDNDD^{54}; see Fig. 3*A*), allowed us to study the importance of hydrophobic interactions made with PcrH for PopD functionality. We also constructed a second CHA mutant strain carrying mutations in the PopD ^{49}VELNAPR^{55} region in which the charges within/around the motif were modified, but its hydrophobic character was maintained (^{49}VRLAAPE^{55}). Plasmids expressing the mutant *pcrH-popBD* section of the operon were introduced individually into the *P. aeruginosa* CHA strain carrying deletions of *popB* and *popD* (Δ*popBD*) (28), and expression and secretion capabilities of the resulting strains, as well as their cytotoxicity toward macrophages, were tested.

P. aeruginosa strains expressing PopD variants carrying ^{49}DEDNDD^{54} or ^{49}VRLAAPE^{55} in lieu of the wild type sequence (henceforth called PopD-4D and PopD-RAE, respectively) were both able to express PopD variants much like wild type cells (Fig. 4*A*). In addition, their growth rate was also comparable with that of the wild type *Pseudomonas* strain (data not shown). *P. aeruginosa* PopD-RAE was able to secrete the mutant form of PopD at wild type levels and caused macrophage lysis at levels that were only slightly lower than wild type cells (Fig. 4*B*), indicating that modification of charges/polarity of the PopD ^{49}VELNAP^{54} motif has very little effect on T3SS functionality. Notably, however, *P. aeruginosa* PopD-4D was unable to secrete PopD at any detectable levels (Fig. 4*A*); in addition, its cytotoxicity toward macrophages was dramatically different from the wild type strain, being comparable with the one presented by the *Pseudomonas* strain lacking PopB and PopD altogether (Δ*popBD*; Fig. 4*B*). To verify if, in the PopD-4D strain, the inability of PopD to be secreted was a consequence of its intracellular instability, we grew *P. aeruginosa* PopD-4D and PopD-RAE cells in conditions that allowed induction of the T3SS by Ca^{2+} depletion, and we subsequently blocked protein synthesis by the addition of chloramphenicol. Samples were then taken at different time points, and results were analyzed by Western blots with anti-PopD antibodies. As shown in Fig. 4*C*, although wild type and PopD-RAE *P. aeruginosa* strains displayed stable forms of PopD, the PopD-4D strain could not stably maintain the PopD variant within the cytoplasm. Because the disruption of chaperone-partner complexes in

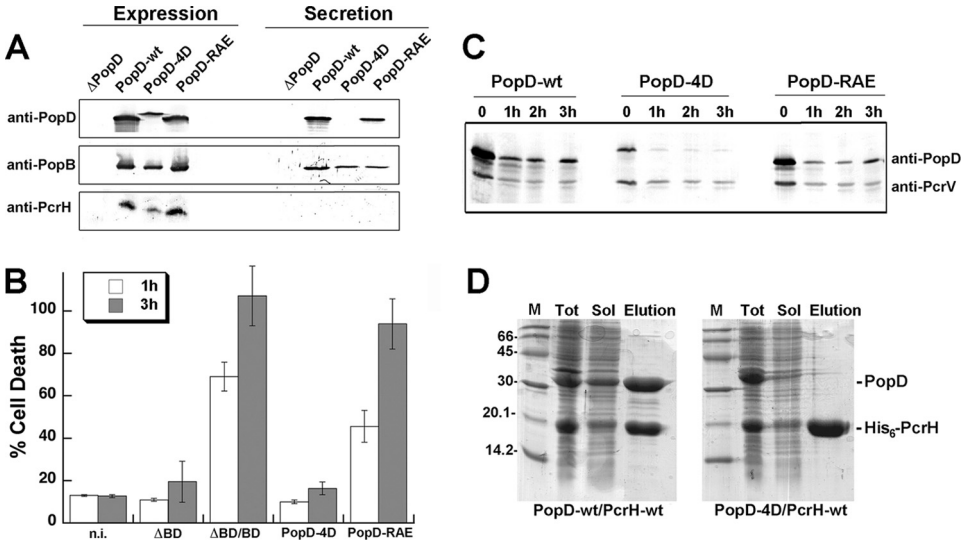

FIGURE 4. *A, Pseudomonas* Δ*popBD* cultures or complemented by plapG-*pcrHpopBD* carrying either *popDwt*, *popD-4D*, or *popD-RAE* were grown in T3SS-induced conditions (see "Experimental Procedures"). The protein content of both pellet (*expression*) and supernatant (*secretion*) were analyzed by Western blotting. *B,* capacity of the PopD mutants to lyse macrophages was measured by the quantification of lactate dehydrogenase release. Noninfected cells (*n.i*) were used as negative controls. All values are the average of four measurements. *C,* stability of PopD mutants was tested with the same culture conditions as for *A*. At $A_{600\ nm} = 1$ A.U., protein synthesis was interrupted by the addition of chloramphenicol, and protein stability was checked at 1–3 h and analyzed by Western blotting. Expression of PcrV was used as a positive control. *D,* interaction between PcrH and PopD was analyzed by co-purification on a HisTrap column. *E. coli* cultures expressing both His_6-PcrH/PopDwt or His_6-PcrH/PopD-4D (*Tot*) were lysed, and the soluble fractions (*Sol*) were applied onto a HisTrap column. Proteins bound to the column were eluted with a linear gradient of imidazole (*Elution*). Only PopDwt co-eluted with His_6-PcrH. The different purification steps were analyzed by SDS-PAGE 15% and colored by Coomassie Blue stain. *Lane M,* molecular weight marker.

T3SS has been shown to lead to target molecule instability in the bacterial cytoplasm (13, 15, 29, 30), we hypothesized that the PopD ^{49}DEDNDD^{54} variant expressed by PopD-4D, in which Val-49, Leu-51, Ala-53, and Pro-54 have all been mutated to Asp, could not be stabilized by PcrH and was thus rapidly degraded. These results strongly suggest that the hydrophobic residues in PcrH-recognition motif of PopD play key roles in the stability and fold of the PopD translocator protein.

To confirm this result *in vitro*, we constructed a bicistronic system that allowed us to express and purify PopD-4D concomitantly with PcrH, the latter harboring a His_6 tag, from the *E. coli* cytoplasm. After induction of protein synthesis, we tested if the purified proteins remained associated in Ni^{2+}-chelating chromatography (Fig. 4*D*). Contrary to wild type PopD, which remains associated to PcrH with 1:1 stoichiometry after Ni^{2+} column chromatography and elution in imidazole buffer, PopD-4D was unable to remain associated to PcrH through the purification; in addition, it was less present in the soluble fraction of the *E. coli* cytoplasmic extract. These observations thus confirm that ^{49}VELNAP^{54} is a key PcrH association motif in minor translocon protein PopD, being stabilized through hydrophobic interactions that play essential roles in T3SS-induced infectivity.

DISCUSSION

Formation of the translocon, a proteinaceous pore inserted in the eukaryotic target membrane, is one of the initial, essential steps that will allow T3SS effector injection directly into the host cytoplasm. The translocon is composed of one hydrophilic and two hydrophobic translocator proteins (6). The hydrophilic member of the translocon has been shown to associate to the tip of the T3SS needle (31–33). The study of the hydrophobic translocators, however, has been challenging, not only due to their membranous character but also to their multistructural aspects, which include: 1) requirement for chaperone release prior to transit through the T3SS; 2) unfolding to allow passage through the needle; and 3) refolding, oligomerization, and interaction with the target membrane once on the surface of the eukaryotic cell. These structural modifications require that the translocators be at least partly in molten globular form both in the presence and absence of chaperone (27).

In the bacterial cytoplasm and prior to T3S-induced secretion, the two hydrophobic translocators exist associated to the same chaperone. PcrH exists in equilibrium between monomeric and dimeric species in the absence of substrate (a behavior shared by its *Yersinia* counterpart, SycD (16)) but is stabilized as a monomer once bound to PopD. The high resolution structure of PcrH reveals a 7-helical TPR fold, which is shared not only by the translocator chaperones SycD and IpgC but also by chaperones of the T3SS needle proteins, shown to stabilize the needle building block within the concave region of the TPR domain (18, 34). This is in stark contrast to structures of chaperones of T3SS effectors, which display mixed α/β folds and, in many cases, share structural similarities even though they recognize distinct effectors from different bacterial species (35–38). This observation suggests that there is potentially a strict structural conservation of chaperones of "early" substrates, such as needle-forming and translocon components, likely reflecting not only the necessity of functional interaction with other components of the T3SS (such as the ATPase or other elements of the base, prior to secretion), but also possibly participating in the regulation of secretion order. Thus, it is tempting to propose that structural components of the T3SS that must be secreted to ensure system functionality are stabilized within the cytoplasm by TPR-like chaperones, whereas toxins, secreted only once the T3SS is fully formed, are recognized by chaperones with non-TPR folds. This hypothesis is in agreement with the idea that chaperone-partner complexes could act as three-dimensional secretion signals (10, 36) and suggests that the fold of the cognate chaperone may be one of the mechanisms involved in the determination of the hierarchy of target protein translocation.

T3SS translocator chaperones, whose molecular mass is in the range of 18 kDa, must thus recognize two distinct substrates

with at least twice that mass. The high resolution structure of PcrH in complex with a peptide from the N terminus of the single transmembrane translocator PopD, described in this work, reveals that the concave region of the chaperone is occupied by the translocator. This result displays analogy to the structure of the IpgC TPR-like chaperone complexed to a highly similar peptide from the major translocator IpaB, which reveals a very similar positioning of peptide in the palm of the TPR-like fold. Thus, type II T3SS chaperones employ their concave region to bind both types of translocator proteins. These results thus suggest that the formation of a ternary complex between the chaperone and the two translocator molecules, which would in principle involve the existence of distinct binding regions for the two translocators on the same chaperone molecule, is highly improbable; instead, they indicate the formation of two different binary complexes, in which the concave region of the chaperone is employed for a similar function in both cases.

This was an unexpected result, in light of mutational analysis of PcrH, which predicted that the cleft of the chaperone would be involved in binding the major translocator (PopB), whereas the convex face contained the binding site for the minor translocator (PopD) (14). This potential discrepancy, however, can be explained by the structure of the PcrH-PopD complex presented here. PcrH residues whose mutagenesis by Bröms *et al.* (14) compromised expression and secretion of both PopB and PopD are shown in *yellow* in Fig. 5*A*; residues whose mutagenesis compromised expression and secretion uniquely of PopB are depicted in *magenta*. The PopD peptide is shown as a *green ribbon* in Fig. 5*A*. It is notable that residues that are closer to the PopD peptide affect both PopB and PopD binding; this was to be expected if the first three helices of PcrH were involved in binding similar N-terminal peptides from both PopB and PopD. Interestingly, Edqvist *et al.* (13), by performing site-specific mutagenesis experiments on SycD, with which PcrH shares 59.7% sequence identity, identified that residues Leu-42, His-67, and Leu-76 play key roles in YopD expression and secretion. His-67 is located between H2 and H3, whereas Leu-42 and Leu-76 are both in the convex region of the chaperone. Considering the fact that PopD maintains a molten globule character even while bound to PcrH (27), it is conceivable that the 47–55-region of PopD be recognized in the concave region of PcrH, and the rest of the protein remains wrapped around the chaperone, involving residues of the convex region. Similarly, it is tempting to propose that once PopB is bound to PcrH, the concave region is employed to secure an N-terminal peptide, and the rest of the molecule (~390 residues) will wrap around PcrH, contacting residues located on the H4 helix of PcrH for stabilization. It is of interest that mapping of conserved residues of type II chaperones from different pathogenic species ranging from *Yersinia pestis* to *E. coli* on the surface of PcrH reveals that it is mostly the first half of the chaperone, including the concave region and the top of the convex section, that has the highest concentration of conserved residues (Fig. 5*B*), suggesting that the C-terminal half of the molecule could be involved in other T3SS-related functions.

The most remarkable result of this work involves the analysis of the behavior of infectious *P. aeruginosa* strains carrying

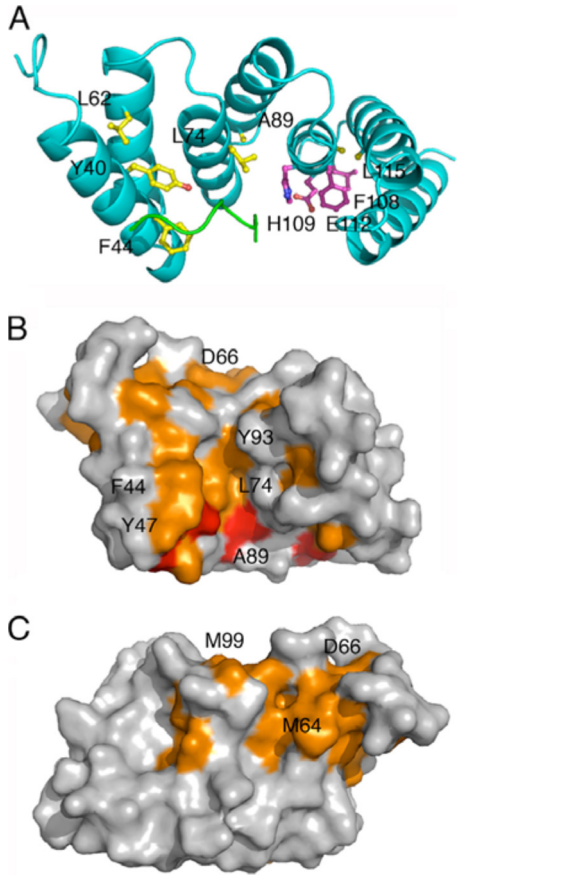

FIGURE 5. **PcrH mutant analysis and surface conservation.** *A,* mapping of the residues mutated by Bröms *et al.* (14) on the surface of PcrH reveals that mutations that affected both PopB and PopD binding (*yellow*) are mostly located on the N-terminal region of the chaperone, whereas mutations that affect only PopB recognition (*magenta*) are mostly located on H5. PcrH from *P. aeruginosa* strain CHA contains one less amino acid on its N terminus than that from strain PAO1 or *Yersinia* SycD; thus, by comparison with these molecules, the numbering differs by 1. *B,* surface mapping of conserved (*orange*) and identical (*red*) amino acids in type II chaperone sequences of T3SS in *P. aeruginosa*, *E. coli*, *Salmonella typhimurium*, *S. flexneri*, and *Y. pestis*. *C,* same as *B*, but from a 180° perspective. The concave region of the TPR "hand" is highly conserved, but the *top part* of the convex region also displays considerable conservation.

mutations on a short stretch of the PopD translocator. Mutation of the hydrophobic anchors, but not of the polar residues located within the same sequence, abolishes cytotoxicity of a clinical isolate toward macrophages. This provides evidence of the subtle sensitivity displayed by the T3SS toward stability of specific protein-protein interaction regions, as observed previously for the T3SS needle formation complex (18), and confirms that certain complexes of the T3SS can be exploited as novel, potential antibiotic development targets.

Acknowledgments—We thank the staff of ESRF beamlines ID14-EH2 and EH4 for help with data collection, Carlos Contreras-Martel (Institut de Biologie Structurale) for help with structure refinement, and J. Marquez and the HTX laboratory team (Partnership for Structural Biology) for access to and help with high throughput crystallization.

REFERENCES

1. Cornelis, G. R. (2006) *Nat. Rev. Microbiol.* **4,** 811–825
2. Kimbrough, T. G., and Miller, S. I. (2000) *Proc. Natl. Acad. Sci. U.S.A.* **97,**

11008–11013
3. Marlovits, T. C., Kubori, T., Lara-Tejero, M., Thomas, D., Unger, V. M., and Galán, J. E. (2006) *Nature* **441,** 637–640
4. Kubori, T., Sukhan, A., Aizawa, S. I., and Galán, J. E. (2000) *Proc. Natl. Acad. Sci. U.S.A.* **97,** 10225–10230
5. Blocker, A., Jouihri, N., Larquet, E., Gounon, P., Ebel, F., Parsot, C., Sansonetti, P., and Allaoui, A. (2001) *Mol. Microbiol.* **39,** 652–663
6. Mueller, C. A., Broz, P., and Cornelis, G. R. (2008) *Mol. Microbiol.* **68,** 1085–1095
7. Büttner, D., and Bonas, U. (2002) *Trends Microbiol.* **10,** 186–192
8. Troisfontaines, P., and Cornelis, G. R. (2005) *Physiology* **20,** 326–339
9. Galán, J. E. (2009) *Cell Host Microbe* **5,** 571–579
10. Ghosh, P. (2004) *Microbiol. Mol. Biol. Rev.* **68,** 771–795
11. Pallen, M. J., Francis, M. S., and Fütterer, K. (2003) *FEMS Microbiol. Lett.* **223,** 53–60
12. Parsot, C., Hamiaux, C., and Page, A. L. (2003) *Curr. Opin. Microbiol.* **6,** 7–14
13. Edqvist, P. J., Bröms, J. E., Betts, H. J., Forsberg, A., Pallen, M. J., and Francis, M. S. (2006) *Mol. Microbiol.* **59,** 31–44
14. Bröms, J. E., Edqvist, P. J., Forsberg, A., and Francis, M. S. (2006) *FEMS Microbiol. Lett.* **256,** 57–66
15. Neyt, C., and Cornelis, G. R. (1999) *Mol. Microbiol.* **31,** 143–156
16. Büttner, C. R., Sorg, I., Cornelis, G. R., Heinz, D. W., and Niemann, H. H. (2008) *J. Mol. Biol.* **375,** 997–1012
17. Lunelli, M., Lokareddy, R. K., Zychlinsky, A., and Kolbe, M. (2009) *Proc. Natl. Acad. Sci. U.S.A.* **106,** 9661–9666
18. Quinaud, M., Plé, S., Job, V., Contreras-Martel, C., Simorre, J. P., Attree, I., and Dessen, A. (2007) *Proc. Natl. Acad. Sci. U.S.A.* **104,** 7803–7808
19. Dacheux, D., Goure, J., Chabert, J., Usson, Y., and Attree, I. (2001) *Mol. Microbiol.* **40,** 76–85
20. Schoehn, G., Di Guilmi, A. M., Lemaire, D., Attree, I., Weissenhorn, W., and Dessen, A. (2003) *EMBO J.* **22,** 4957–4967
21. Faudry, E., Vernier, G., Neumann, E., Forge, V., and Attree, I. (2006) *Biochemistry* **45,** 8117–8123
22. Kabsch, W. (1993) *J. Appl. Crystallogr.* **26,** 795–800
23. McCoy, A. J., Grosse-Kunstleve, R. W., Adams, P. D., Winn, M. D., Storoni, L. C., and Read, R. J. (2007) *J. Appl. Crystallogr.* **40,** 658–674
24. Murshudov, G. N., Vagin, A. A., and Dodson, E. J. (1997) *Acta Crystallogr. D Biol. Crystallogr.* **53,** 240–255
25. Emsley, P., and Cowtan, K. (2004) *Acta Crystallogr. D Biol. Crystallogr.* **60,** 2126–2132
26. Davis, I. W., Leaver-Fay, A., Chen, V. B., Block, J. N., Kapral, G. J., Wang, X., Murray, L. W., Arendall, W. B., 3rd, Snoeyink, J., Richardson, J. S., and Richardson, D. C. (2007) *Nucleic Acids Res.* **35,** W375–W383
27. Faudry, E., Job, V., Dessen, A., Attree, I., and Forge, V. (2007) *FEBS J.* **274,** 3601–3610
28. Goure, J., Pastor, A., Faudry, E., Chabert, J., Dessen, A., and Attree, I. (2004) *Infect. Immun.* **72,** 4741–4750
29. Quinaud, M., Chabert, J., Faudry, E., Neumann, E., Lemaire, D., Pastor, A., Elsen, S., Dessen, A., and Attree, I. (2005) *J. Biol. Chem.* **280,** 36293–36300
30. Creasey, E. A., Delahay, R. M., Bishop, A. A., Shaw, R. K., Kenny, B., Knutton, S., and Frankel, G. (2003) *Mol. Microbiol.* **47,** 209–221
31. Mueller, C. A., Broz, P., Müller, S. A., Ringler, P., Erne-Brand, F., Sorg, I., Kuhn, M., Engel, A., and Cornelis, G. R. (2005) *Science* **310,** 674–676
32. Espina, M., Olive, A. J., Kenjale, R., Moore, D. S., Ausar, S. F., Kaminski, R. W., Oaks, E. V., Middaugh, C. R., Picking, W. D., and Picking, W. L. (2006) *Infect. Immun.* **74,** 4391–4400
33. Deane, J. E., Roversi, P., Cordes, F. S., Johnson, S., Kenjale, R., Daniell, S., Booy, F., Picking, W. D., Picking, W. L., Blocker, A. J., and Lea, S. M. (2006) *Proc. Natl. Acad. Sci. U.S.A.* **103,** 12529–12533
34. Sun, P., Tropea, J. E., Austin, B. P., Cherry, S., and Waugh, D. S. (2008) *J. Mol. Biol.* **377,** 819–830
35. Luo, Y., Bertero, M. G., Frey, E. A., Pfuetzner, R. A., Wenk, M. R., Creagh, L., Marcus, S. L., Lim, D., Sicheri, F., Kay, C., Haynes, C., Finlay, B. B., and Strynadka, N. C. (2001) *Nat. Struct. Biol.* **8,** 1031–1036
36. Birtalan, S. C., Phillips, R. M., and Ghosh, P. (2002) *Mol. Cell* **9,** 971–980
37. Lilic, M., Vujanac, M., and Stebbins, C. E. (2006) *Mol. Cell* **21,** 653–664
38. Stebbins, C. E., and Galán, J. E. (2001) *Nature* **414,** 77–81
39. DeLano, W. L. (2002) *The PyMOL Molecular Graphics System,* Ver. 1.2r3pre, Schrödinger, LLC, San Diego, CA